

Raman Vibrational Signatures of Excited States of Echinenone in the Orange Carotenoid Protein (OCP) and Implications for its Photoactivation Mechanism

Petra Chrupková^{1,2}, Ivo H. M. van Stokkum³, Thomas Friedrich⁴, Marcus Moldenhauer⁴, Nediljko Budisa⁵, Hsueh-Wei Tseng⁵, Tomáš Polívka², Dmitry A. Cherepanov^{6,7}, Eugene G. Maksimov⁸ and Miroslav Klož^{1*}

1 - The Extreme Light Infrastructure ERIC, ELI Beamlines Facility, Za Radnicí 835, Dolní Břežany, Czech Republic

2 - University of South Bohemia in České Budějovice, Faculty of Science, Branišovská 1760, 370 05 České Budějovice, Czech Republic

3 - Vrije Universiteit, Department of Physics and Astronomy, Faculty of Sciences, De Boelelaan 1081, 1081HV Amsterdam, the Netherlands

4 - Technische Universität Berlin, Institute of Chemistry PC 14, Straße des 17. Juni 135, 10623 Berlin, Germany

5 - University of Manitoba, Department of Chemistry, 144 Dysart Rd, 360 Parker Building, Winnipeg, MB R3T 2N2, Canada

6 - N.N. Semenov Federal Research Center for Chemical Physics, Russian Academy of Sciences, 142432 Moscow, Russian Federation

7 - Lomonosov Moscow State University, A.N. Belozersky Institute of Physical-Chemical Biology, 119991 Moscow, Russian Federation

8 - Lomonosov Moscow State University, Faculty of Biology, Vorobyovy Gory 1-12, Moscow 119991, Russian Federation

Correspondence to Miroslav Klož: miroslav.kloz@eli-beams.eu (M. Klož)

<https://doi.org/10.1016/j.jmb.2024.168625>

Edited by Volha Chukhutsina

Abstract

In this study, the vibrational characteristics of optically excited echinenone in various solvents and the Orange Carotenoid Protein (OCP) in red and orange states are systematically investigated through steady-state and time-resolved spectroscopy techniques. Time-resolved experiments, employing both Transient Absorption (TA) and Femtosecond Stimulated Raman Spectroscopy (FSRS), reveal different states in the OCP photoactivation process. The time-resolved studies indicate vibrational signatures of excited states positioned above the S_1 state during the initial 140 fs of carotenoid evolution in OCP, an absence of a vibrational signature for the relaxed S_1 state of echinenone in OCP, and more robust signatures of a highly excited ground state (GS) in OCP. Differences in S_1 state vibration population signatures between OCP and solvents are attributed to distinct conformations of echinenone in OCP and hydrogen bonds at the keto group forming a short-lived intramolecular charge transfer (ICT) state. The vibrational dynamics of the hot GS in OCP show a more pronounced red shift of ground state C=C vibration compared to echinenone in solvents, thus suggesting an unusually hot form of GS. The study proposes a hypothesis for the photoactivation mechanism of OCP, emphasizing the high level of vibrational excitation in longitudinal stretching modes as a driving force. In conclusion, the comparison of vibrational signatures reveals unique dynamics of energy dissipation in OCP, providing insights into the photoactivation mechanism and highlighting the impact of the protein environment on carotenoid behavior. The study underscores the importance of vibrational analysis in understanding the intricate processes involved in early phase OCP photoactivation.

© 2024 The Author(s). Published by Elsevier Ltd. This is an open access article under the CC BY license (<http://creativecommons.org/licenses/by/4.0/>).

Introduction

One of the pivotal mechanisms governing the functionality of living organisms resides in the ability to create localized, confined environments that selectively facilitate desired chemical reactions. Among these, the protein-matrix stands out as a fundamental locale. Within the confines of the binding pocket, a substrate can be intricately bound, leading to a substantial enhancement in reaction rates or the acquisition of unusual functional properties by certain cofactors. An illustrative instance of this phenomenon is exemplified by the orange carotenoid protein (OCP), which functions as a keto-carotenoid-binding protein and yet remains the only carotenoid protein that manifests photoactivation^{1–3} (Figure 1).

Orange Carotenoid Protein type 1 (OCP or OCP1) is a unique photoprotective, water-soluble protein predominantly found in cyanobacteria. It plays a critical role in non-photochemical quenching (NPQ), a protective process that dissipates excess absorbed light energy as heat,

safeguarding photosynthetic organisms from photodamage.^{2,4} The photoactivation of OCP is enabled through the absorption of blue-green light by incorporated carbonyl carotenoids such as echinenone, 3'-hydroxyechinenone, or canthaxanthin.⁵ OCP operates in cyanobacteria, interacting with phycobilisome to mitigate energy transfer to the photosystems and neutralize reactive singlet oxygen radicals.⁶ This function is crucial for cyanobacteria in environments with fluctuating light conditions, allowing them to maximize photosynthesis efficiency while reducing stress from intense light exposure.^{2,7}

The OCP1 protein is the most prevalent form within the OCP protein family, with OCP2 and OCP3 being more recently identified and less understood in terms of their structure and function.^{8,9} However, a recent study⁹ has shed light on these proteins, revealing that they possess distinct structural characteristics compared to OCP1. Additionally, they demonstrate varied affinities towards phycobilisomes, which results in a lower quenching efficiency than the evolutionary more optimized OCP1. From now on, in the text we will

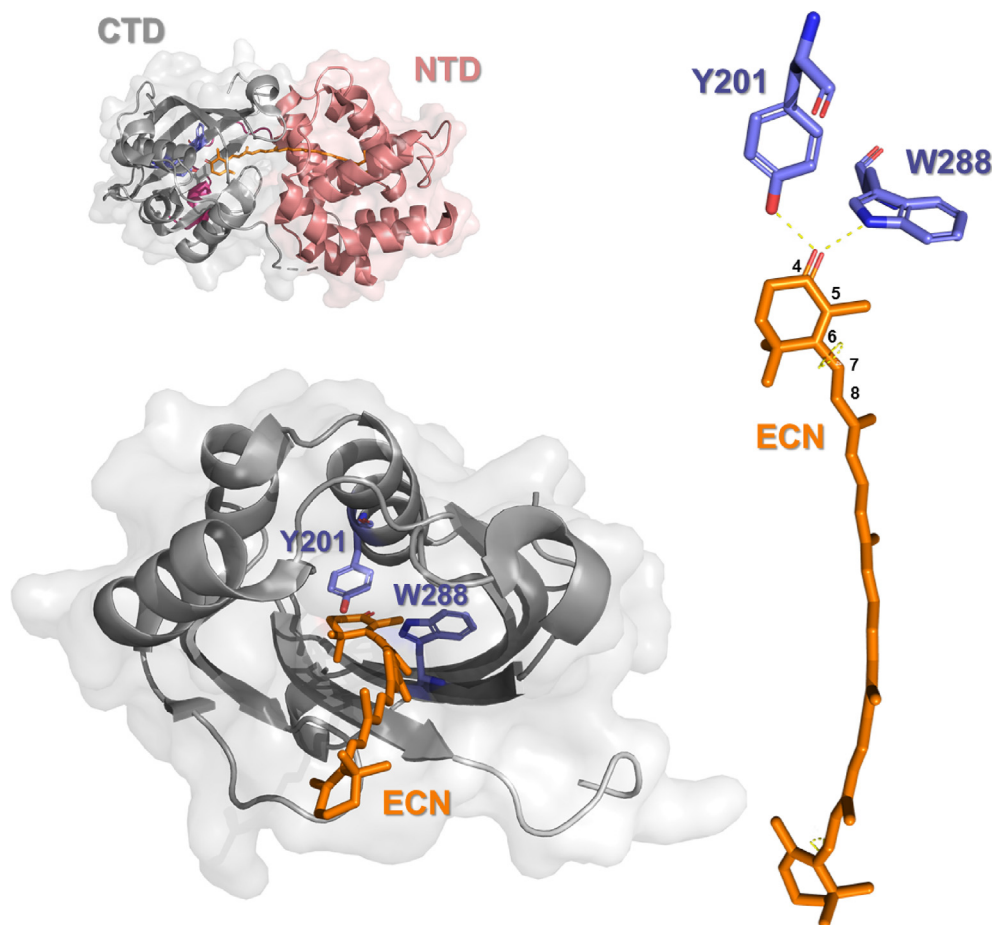


Figure 1. The overall structure of the OCP protein (PDB ID 3MG1) shown from the side (top) and through the carotenoid binding cavity (bottom) with a non-planar configuration of echinenone in the binding pocket with hydrogen bonds visualized (right).

use the abbreviation OCP to denote the OCP1 protein that we have studied.

Orange Carotenoid Proteins (OCPs) are also attracting interest beyond the photosynthetic world, due to their unique features such as structural modularity, responsiveness to environmental changes, and light-activated transformations, promising innovative applications in bioengineering and synthetic biology.¹⁰ Beyond photoprotection, the photo-switching activity of OCPs enables diverse applications, ranging from gene regulation in chloroplasts¹¹ to modulating excitation energy transfer between fluorescent dyes in artificial light-harvesting systems.¹² Additionally, OCPs serve as precise sensors for detecting environmental pH variations¹³ and temperature changes,¹⁴ offering accurate detection capabilities down to the cellular level. They also enhance carotenoid bioavailability and antioxidant delivery, either through their hydrophilicity or when immobilized on nanoparticles, showing promise for drug delivery systems¹⁵ and optical nanodevices.¹⁶

The OCP protein in its inactive “orange form” (OCPo) is composed of two distinct amino acid domains: the N-terminal domain (NTD) and the C-terminal domain (CTD). In OCPo these domains are closely interconnected, predominantly through hydrogen bonding. The presence of a centrally located carotenoid molecule, acting as a bridge, significantly mediates interaction between the two domains. Within the NTD, the carotenoid chain is securely anchored through a series of interactions, including hydrophobic interactions, hydrogen bonding of the keto group, and van der Waals forces, stabilizing it within a hydrophobic pocket. Conversely, the interaction of the carotenoid with the CTD is chiefly characterized by hydrogen bonds formed between the carotenoid’s carbonyl group and two specific amino acids: tyrosine (Tyr201) and tryptophan (Trp288),^{2,17,18} which are believed to be the initial points of OCP protein activation. Subsequent to exposure to blue/green light, these hydrogen bonds are disrupted, leading to a transition of the OCP into the “Red state” (OCP_r), so named due to its red appearance caused by red shift of the absorbance spectrum with concomitant loss of vibrational structure.^{2,19} In this altered state, the NTD and CTD units get separated while the carotenoid enters NTD,^{19–22} allowing the protein to bind with the phycobilisome,²³ a light-harvesting antenna found in cyanobacteria. This interaction triggers the nonphotochemical quenching of the antenna, transitioning it into a photoprotective mode. Although the crystal structure of OCP from *Synechocystis* is characterized by the presence of two hydrogen bonds (Figure 1), comparison of the spectral characteristics of this sample and a number of mutants,^{24–27} as well as representatives of other families of OCP,⁹ indicate a significant heterogeneity of the dark-adapted state associated with the possibility of

spontaneous disruption of either one or both of the two hydrogen bonds.

The photoactivation process itself is subject of ongoing debate, with three primary hypotheses proposed: 1. The initial step in OCPo activation is the rupture of hydrogen bonds between the keto group and amino acids in the C-terminal domain (CTD).^{19,22,28–31} 2. The initial step involves a different mechanism as some form of isomerization, yet to be fully elucidated,³² or 3. the potential formation of the oxocarbenium cation can be a precursor for hydrogen bond breakage.²⁴ Crucially, in all theories, the rupture of hydrogen bonds, leading to domain dissociation, is a common outcome. The distinction lies in whether the bond rupture directly results from carotenoid excitation or is secondary to other more substantial molecular changes. A recently published study also offers a new perspective on the initial activation of the protein, stating that the first change in the protein is the dissociation of the dimer into two OCP monomers.³³

The discussion of OCPo activation related to carotenoid isomerization and its detection yields contradictory conclusions. Some studies challenge the occurrence of isomerization, proposing various explanations that isomerization does not occur during the protein activation.^{2,24,34} Conversely, the study by Leverenz et al. (2015) suggests isomerization of the C6–C7 single bond, which is at the side of the β 1-ring position.¹⁹ Another study³² employing a crystallography diffraction experiment, presents an evidence of isomerization from s-trans to cis-trans at the C9’–C8’ single bond simultaneously with a s-cis to s-trans change between the C7’–C6’ single bond, adjacent to the part of the carotenoid closer to the NTD unit. This finding reveals a unique dynamic where hydrogen bond rupture is not the triggering cause of activation but rather a consequence of preceding isomerization changes.

The discrepancies between these studies can be attributed to the inherent challenges in detecting carotenoid isomerization through standard spectroscopic methods like steady state Resonance Raman spectroscopy,^{2,34} Transient Absorption Spectroscopy (TA),^{1,24,29} and Fourier transform infrared spectroscopy (FTIR).^{5,35}

Furthermore, the low quantum yield of photoactivation, repeatedly reported substantially below 1%,^{2,29,31,36} potentially an evolutionary adaptation for high-light conditions sensing, presents another obstacle. This low yield is exacerbated by the ultrashort pulse approach commonly used in spectroscopic experiments, which often proves insufficient for generating a detectable population of activated OCP. This issue of low quantum efficiency is addressed in other time-resolved experiments (FTIR^{5,29,32} or X-ray protein crystallography³²) by using a continuous light source or flash lamps that allows multiple re-excitations and photoproduct accumulation. The subsequent dynamics of the formation of individual intermediate

states (associated with protein conformational changes, units' dissociation) are often slowed down by the low temperature of the experiment due to low time resolution and the need for high acquisition time or due to the nature of the experiment itself, such as in experiments on the crystalline form of the protein. However, all these methods provide little information about potential changes within the excited states of carotenoids. We believe that ultra-fast spectroscopic methods, such as Femtosecond-Stimulated Raman Spectroscopy (FSRS), can fill the gap in missing information because, even though the method may not lead to complete deciphering of OCP photoactivation, it can reveal pathways that energy from the absorbed photon follows. Thus, studying energy dissipation pathways in OCPo could reveal potential activation mechanisms, despite the dynamics of the photoproduct itself not being directly observable in its entirety.

Intriguingly, in OCP, carotenoids seem to perform an illumination detection function,² diverging from their traditional roles in light harvesting or photoprotection. The ability of carotenoids to capture, release, or dissipate energy stems from their unique properties in an excited state (ES), originating in the polyene backbone structure with alternating single and double bonds. The ES structure can be described using a basic model, including an accessible singlet state known as S_2 ³⁷ and a dark state called S_1 ³⁸⁻⁴⁰ (Figure 2A). When carotenoids absorb a photon, they are excited to the S_2 state, lasting only on the femtosecond scale before shifting to the lower-lying dark S_1 state. Both the S_2 and S_1 states can transfer energy to the ES of other molecules, like chlorophylls, if they are in a favorable position and are energetically matched.^{39,41} However, if this doesn't occur, the energy dissipates

quickly through a nonradiative mechanism, causing the carotenoid to return to its ground state (GS), releasing the energy into the surroundings as heat.³⁹

Keto-carotenoids like peridinin,⁴² fucoxanthin,⁴³⁻⁴⁵ or the mentioned echinenone^{1,46,47} reveal the presence of additional ESs within the ES manifold, which is depicted in Figure 2B. One of them is known as the intramolecular charge transfer (ICT) state. This state typically appears as a red-shifted extension of the S_1 peak in the TA spectra. This occurs because the keto group pulls electrons from the conjugated chain, creating a distinct ES (or local minimum of the S_1 state).^{46,48,49}

The presence of the ICT state can be intensified in a polar environment, such as a polar solvent like acetonitrile or protic solvents like methanol or a specific protein matrix. Apart from the ICT state, there is a somewhat more mysterious S^* state initially observed as a unique feature in the TA spectra of long homologues of the carotenoid β -carotene.⁵⁰ Unlike the ICT state, the S^* state is not red-shifted from the S_1 state but rather blue-shifted, approaching the GS absorption. Its origin is less well-established than that of the S_1 or ICT states, possibly representing various phenomena leading to absorption slightly red-shifted from the ground GS via different mechanisms.^{8,50-53} Debates persist regarding whether the S^* state is an independent excited state, a local minimum of the S_1 state, or perhaps a form of a non-equilibrated GS.³⁸

Interestingly, echinenone in the OCPo exhibits all these carotenoid states, requiring a more comprehensive model of the carotenoid ES manifold (see Figure 2B).^{29,54,55} Previous TA experiments on the OCPo distinctly reveal features

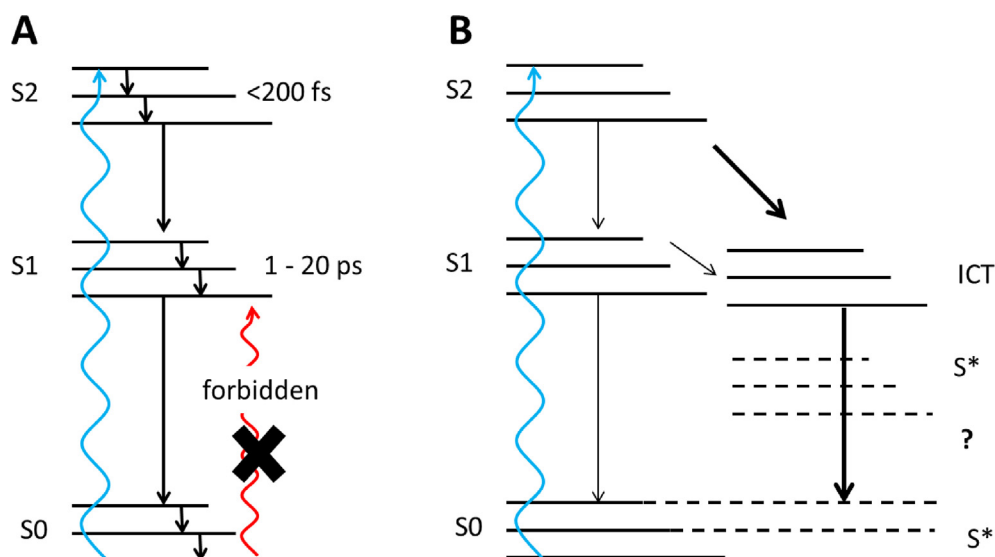


Figure 2. (A) Basic scheme of carotenoid excited state dynamics. (B) Extended scheme of carotenoids ES dynamics, “?” marks controversy regarding the S_1 or S_0 state origin of S^* state phenomena.

associated with both the ICT state and characteristics of the S^* state.²⁹ The pronounced manifestation of the ICT state can be explained by hydrogen bonds on the keto groups and an uneven charge distribution on amino acids around the polyene chain, which enhance such properties in carotenoids.⁵⁶

This study extensively employs vibrational spectroscopy, necessitating an introduction to carotenoid vibrations. Carotenoids are highly symmetric molecules, making backbone modes weak in infrared spectroscopy; however, they are very Raman active. The Raman spectrum of carotenoids is categorized into four main frequency regions, namely ν_1 , ν_2 , ν_3 , and ν_4 . The ν_1 region, representing C=C vibration between 1510 and 1530 cm^{-1} , acts as a signature for the C=C stretch mode. Notably, it experiences a substantial blueshift in higher ES, particularly around 1775 cm^{-1} in the S_1 state and to a lesser extent in the ICT and S_2 states.⁵⁷ The ν_2 band at 1160 cm^{-1} encompasses contributions from stretching vibrations of C—C single bonds coupled with C—H in-plane bending modes, serving as a distinctive feature for carotenoid configurations, especially isomerization states. The ν_3 band at 1000 cm^{-1} arises from in-plane rocking vibrations of methyl groups attached to the conjugated chain, coupled with in-plane bending modes of adjacent C—H's, functioning as a signature for the conjugated end-cycle configuration. The ν_4 band at 960 cm^{-1} results from C—H out-of-plane wagging motions coupled with C=C torsional modes. When the carotenoid conjugated system is planar, these out-of-plane modes are uncoupled from the electronic transition, rendering these bands non-Raman active. However, distortions around C—C single bonds increase the coupling, intensifying the ν_4 band and indicating a backbone twist.^{34,58,59} Such deviations from the planar configuration are characteristic of the carotenoid in the dark-adapted OCPo due to the close interaction with the protein matrix causing end-ring rotation and polyene chain distortion.⁹

In exploring the dynamic behavior of carotenoids in ESs, ultrafast vibrational spectroscopy, particularly FSRS, plays a pivotal role. Traditional Raman scattering, due to its weak signals and susceptibility to luminescence interference, prompted the development of ultrafast techniques like FSRS. Originating from the early 2000s, FSRS emerged as a powerful tool to enhance the time resolution of Raman experiments.⁶⁰ FSRS involves the use of picosecond Raman pump pulses overlapped with femtosecond white light continuum probe pulses. FSRS bears similarities to TA spectroscopy in its experimental realization. This means that the signal is recorded as amplification or absorption of the probe pulse, leading to Raman gain or Raman loss, respectively.⁶¹

The information obtained by the FSRS technique is, in principle, the same as what would be obtained by Raman scattering, but with one distinction. In FSRS experiments, the anti-Stokes region, typically dominated by Raman loss, originates in Stokes-like scattering but provides insights into different resonance regions than the Stokes region.⁶² This paper details FSRS experiments using a 790-nm Raman pump pulse, observing both Stokes and anti-Stokes regions. Effectively, the Stokes region probes resonances at 790 nm, and the anti-Stokes region, probing resonance around 700 nm, complements the Stokes signal, offering a comprehensive view of carotenoid ESs. For the excited states discussed in this paper the Raman pump wavelength can be considered pre-resonant meaning that signal is already enhanced by electronic resonance but cannot be considered fully resonant. The exception is the S_2 state which can be considered fully resonant with the Raman pump.

A crucial aspect of FSRS is its ability to resonate not only with excited state absorption but also with stimulated emission, leading to peak reversal. This phenomenon is particularly relevant for the carotenoid S_2 and ICT state (see the chapter “Peak shapes in FSRS spectroscopy” in the [Supporting information](#)).

Simultaneous recording of TA, FSRS Stokes gain, and FSRS anti-Stokes loss in a smart configuration with synchronized detectors provides a comprehensive dataset for each laser shot. This approach maximizes information retrieval from a single excitation pulse and allows for online verification of FSRS probing the same state as determined by prior TA experiments.

Our investigation includes simultaneous TA, FSRS Stokes gain, and FSRS anti-Stokes loss measurements on fs pulse excited echinenone in various solvents and OCPo. Global data analysis establishes a direct link between TA phenomena and molecular vibrational states, shedding light on the intricate dynamics of echinenone in ESs and its role in OCPo activation. The innovative technique of modeling artifacts related to truncated free induction decay in FSRS experiment to be described elsewhere was used for the first time to extract Raman signatures of ultrafast species.

Methods and Materials

The FSRS spectroscopy set-up, employing the spectral watermark method,⁶³ represents an upgraded version compared to that described in previous work.⁶⁴ In this design, two independent 1 kHz chirped pulse amplifiers were employed, both seeded with femtosecond pulses from a shared Ti:sapphire oscillator. Electronic and optical delays were introduced to the seed, enabling the tracing

of processes beyond six nanoseconds, achievable by optical delay alone. To initiate a photoreaction, a 200 nJ, ~50 fs, 480 nm actinic pump (Ap) was generated by an optical parametric amplifier (OPA). Simultaneously, a 1450 nm signal beam from a second OPA system was focused on a moving CaF₂ plate to generate a white light supercontinuum serving as the probe (Pr). The 780–790 nm femtosecond pulses from the second amplifier passed through a home-built pulse shaper, creating a series of frequency-locked picosecond pulses as the Raman pump (Rp), with an energy of 3 μJ (for a more detailed description see the [Supporting information](#)).

OCPo vs OCPr Raman spectra were recorded by first recording FSRS spectra of the OCP sample without any illumination and then illuminating sample with a 450 nm LED adjusted to a luminal flux of around 1000 μmol/s at the sample until the Raman spectra stopped evolving and then recording FSRS spectra of the activated OCP while illumination was still on.

In the time-resolved study, both TA and FSRS of OCPo were recorded simultaneously for 146 logarithmically spaced delays between Ap and Rp/Pr. A similar experiment with 78 delays was conducted on echinenone in cyclohexane, acetonitrile, and methanol, representing the carotenoid in nonpolar, polar, and polar protic solvents. The experiments in solutions did not thoroughly probe very long delays, as any product persisting over the ps time scale is not considered relevant for understanding OCPo activation. However, the fs and ps scales were measured with identical time sampling of 25 fs as for OCPo. All experiments were conducted under the magic-angle (54.7°) condition to eliminate the influence of orientational relaxation. To minimize the impact of photodamage and photoproduct accumulation in the measurement, the experiment was performed in a flow cell.

Both steady-state and time-resolved absorption, as well as stimulated Raman experiments of OCPo and OCPr, were carried out. For all presented Raman data, both Stokes gain and anti-Stokes loss are plotted as positive. Following the TA convention of absorption being positive and emission or bleach being negative, the graph depicting FSRS in the Stokes region can be considered flipped to visualize Raman gain as positive. Since Stokes Raman gain provides essentially the same information as anti-Stokes Raman loss, and Raman data are usually visualized as positive in literature, such a choice is considered natural. However, in raw data, Stokes and anti-Stokes signals are of opposite sign.

The FSRS experiment used Rp pulses around 790 nm, making the Raman spectra nonresonant with the S₀-S₂ transition of OCPo and mildly pre-resonant with S₀-S₂ transition of OCPr. This pre-resonance is more notable for the anti-Stokes loss

signals than for the Stokes gain signals, which are approximately half in intensity. The reason is that Anti-Stokes data can be considered exploring resonance around 700 nm rather than 790 nm because the probe wavelength, rather than the Rp wavelength, defines the exact resonance. For the critical region of 1500–1800 cm⁻¹ the anti-Stokes Raman loss resonance falls around this wavelength (for details see the “Peak shapes in FSRS spectroscopy” chapter in the [Supporting information](#)).

In the time-resolved studies, both TA and FSRS were simultaneously recorded and analyzed. The resulting kinetics were globally fitted by a 6-compartment sequential model for OCPo and 5-compartment model for echinenone in solvents. Parallel processes were observed, more notably in OCP than in echinenone in solvents. However, in this pioneering work on OCP fs to ps Raman vibrations, a simple sequential model was preferred. This model provides a convenient way to visualize the data, pinpoint key transition processes, and allow comparison of results between OCPo and echinenone in solvents. A notably different target model would be needed for echinenone in solvents and in OCPo, thus obfuscating direct differences in measured data.

Evolution-associated decay spectra (EADS) components with a given time constant closely resemble raw data measured at a given Ap and Pr delay. They benefit from group velocity dispersion (GVD) correction and a better signal-to-noise ratio. This is not the case for target models, where the extracted spectra heavily depend on the model and can differ significantly from structures directly recorded in the experiment. The number of fitted components is based on preliminary data analysis.

For the carotenoid experiment, we used echinenone ≥ 95.0 % (HPLC – 73341), purchased from Merck Life Science. The general appearance and peak positions of measured absorption spectra were consistent with the literature. For dissolution, we used the following solvents: methanol, suitable for HPLC, ≥ 99.9 % (34860); cyclohexane for spectroscopy Uvasol[®] (1.02822); and acetonitrile for spectroscopy Uvasol[®] (1.00016), all purchased from Merck Life Science.

All presented measurements were conducted in 2 mm path length peristaltically pumped flow cuvette on the sample adjusted to optical density 0.7. In case of echinenone in acetonitrile and methanol such concentration was not achievable and experiments were conducted on sample with maximum optical density of 0.15.

To express the OCP from *Synechocystis* sp. PCC 6803, a plasmid was engineered with OCP cDNA, optimized for *E. coli*, and introduced into a modified vector with an N-terminal 6xHis tag. Following IPTG induction and cell harvesting, the

cells were lysed, and the lysate purified through affinity chromatography, ensuring the extraction of a pure protein solution for future applications. More information about OCP production is available in the [supplementary information](#), with a detailed description in the publication by the group that also expresses our protein.⁶⁵

Results

Figure 3 presents absorption spectra of the OCP in the dark and light adapted states and corresponding results of the Raman steady-state experiments. The Raman spectra in the red state show a higher overall magnitude, attributed to the enhanced pre-resonance of the S_0 to S_2 transition at 790 nm Rp, particularly noticeable in the anti-Stokes frame. To illustrate the genuine enhancement of the GS FSRs signal during the OCP conversion from OCPo to OCP_r, non-scaled spectra are plotted in **Figure 3**. Additionally, unscaled difference spectra provide a clearer estimate of the potential photoproduct state's emergence in transient spectra. Detailed and scaled signals associated with the OCPo to OCP_r transition are available in the [Figures S1-2](#) for an in-depth analysis, and also Raman spectra of echinenone in cyclohexane with peak positions indicated can be found in [Figure S3](#).

The spectral peak positions and their mode assignments (ν_1 , ν_2 , ν_3 , and ν_4) are outlined in the introduction and concur with findings in the literature.^{2,34,66} However, we observe subtle differences in peak shapes, with our measurements showing broader peaks. These variations likely result from the differences in measurement techniques (FSRS versus spontaneous Raman spec-

troscopy)⁶⁷ and experimental conditions (nonresonant or mildly pre-resonant in our study as opposed to resonant in others). In line with previous studies, we observe the ν_1 peak shifting from higher to lower energies as the protein transitions from its mostly inactive orange form to the condition where the majority of the population is in the active red state. This shift supports theories of an extended conjugation length in the active form compared to the inactive one. The increase in effective conjugation length during the transition to the red state is usually attributed to the rotation of the ring group and straightening of the polyene chain, which become possible after the hydrogen bonds in the CTD are broken and the carotenoid moves to NTD.

Moreover, we observe changes in peak shapes for modes ν_3 and ν_2 during the transition from OCPo to OCP_r, mirroring findings reported in the literature. Specifically, these changes are reflected in the alteration of peak shapes throughout the transition. Although these modifications in ν_2 modes are subtle and do not allow for definitive conclusions about isomerization, they, combined with the observed alterations in ν_4 mode, suggest that the carotenoid assumes a more planar conformation in its OCP_r state which was also proposed in the study by Wilson et al.²

Next, results from the time-resolved experiment are presented as both TA and FSRs were employed to study OCPo and echinenone in three types of solvents, cyclohexane, methanol, and acetonitrile. The findings, illustrated in [Figures 4–7](#) are plotted in the form of fitted components and their color coding is consistent across figures, aiding cross-reference. More detailed figures with peak position and scales indicating actual signal magnitudes can be found in the [Figures S4–S7](#) and raw data in the [Figures S8–S15](#).

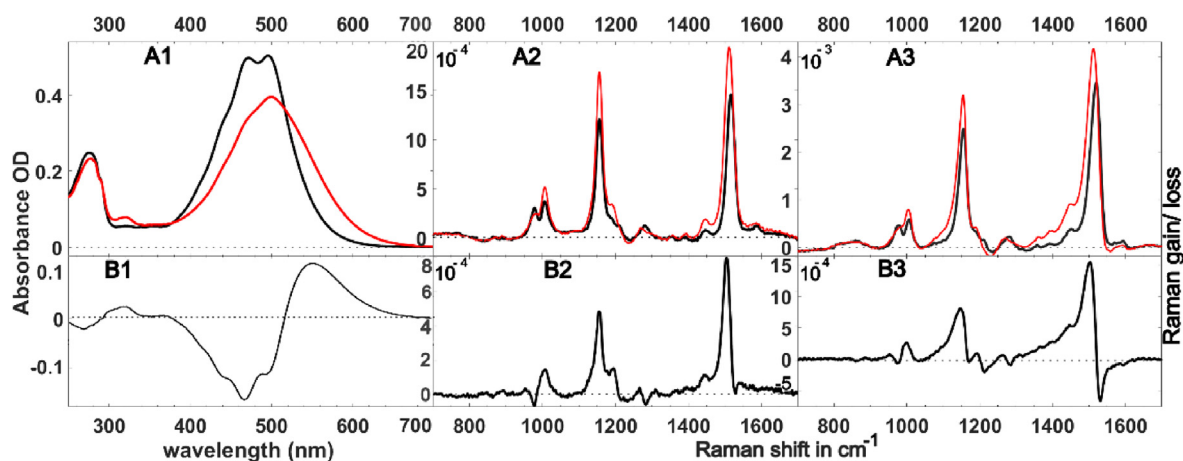


Figure 3. Comparison of steady state spectra (A) of the dark adapted OCP before the illumination (black) and photoactivated form of OCP (red) after the illumination by 450 nm LED light and light-minus-dark state differences (B). A1: absorption spectra, A2: FSRs Stokes Raman spectra, A3: FSRs anti-Stokes spectra, B1: Difference of illuminated OCP minus dark form of OCP absorption, B2: Difference of illuminated OCP minus dark form of OCP of Stokes FSRs, B3: Difference of illuminated OCP minus dark form of OCP anti-Stokes FSRs.

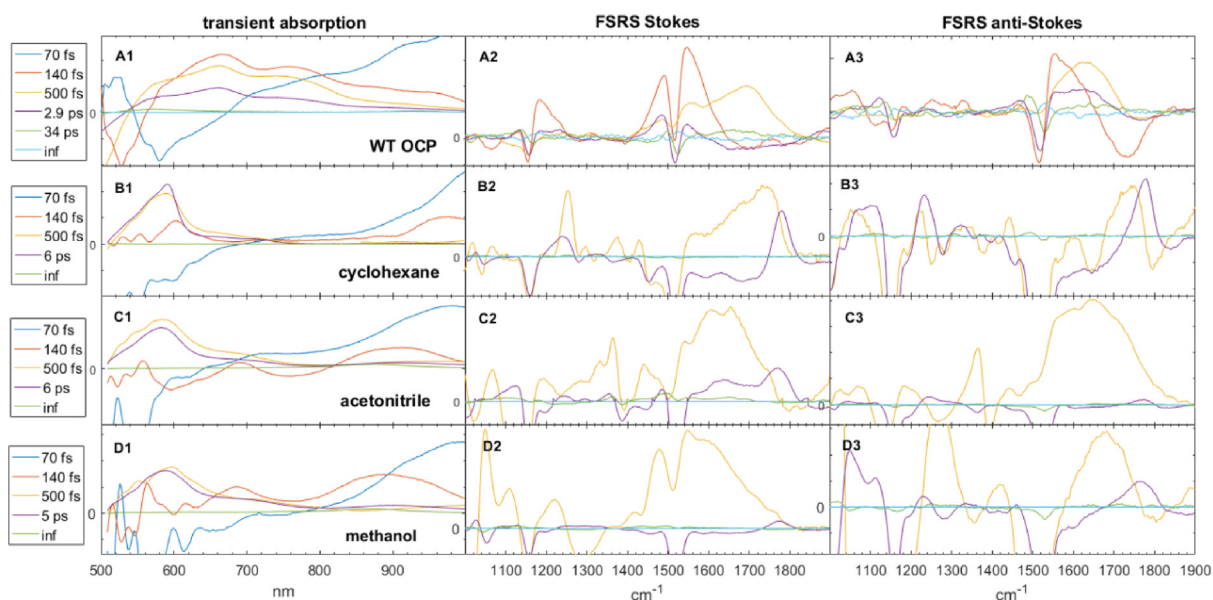


Figure 4. Summary of simultaneous analysis of TA and FSRS data recorded on echinenone in OCP and in various solvents. The 70 fs component is not shown in the FSRS data, the 140 fs and 70 fs FSRS components are not shown in data from echinenone in solvents (cyclohexane, acetonitrile, methanol). Panels A2 and A3 are magnified and annotated in Figure 6.

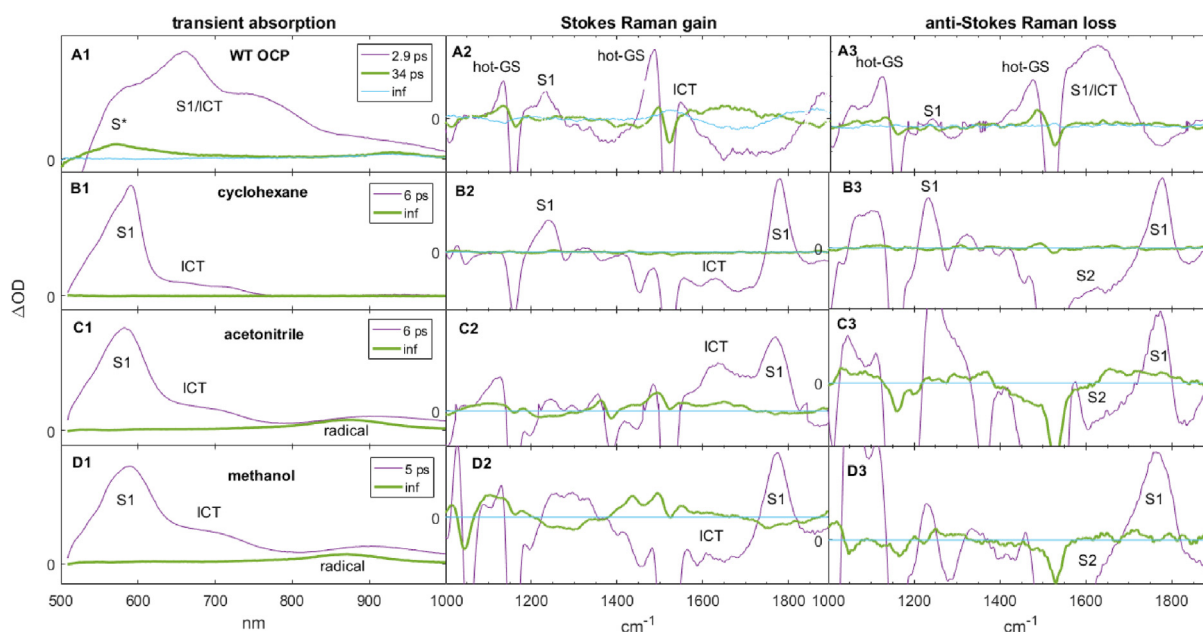


Figure 5. Summary of vibrational dynamics of echinenone in OCP and in solvents (cyclohexane, acetonitrile, methanol) on ps timescale with peak assignment. “S₂” means negative peaks with spurious S₂ state repumping from S₁ ESA. Note the prominence of the S₁ peak in all solvents and its absence in OCPo. This is a magnification of the last two or three EADS from Figure 4, with the addition of the assignments.

The initial data discussed here relate to the TA spectra of echinenone in solvents. The data are shown in the Figure 4 (sub-panels B1, C1 and D1), and the picosecond components are magnified in the Figure 5 (again sub-panels B1, C1 and D1) to better distinguish peaks at ps scale

that are of smaller magnitude than signals at fs scale. TA of echinenone in solvents aligns with studies by Polívka et al. and Chabera et al.^{1,46} For echinenone in a non-polar solvent, the measured kinetics were 70 fs, 140 fs, 500 fs, and 6 ps, with the main peak at 6 ps associated with the S₁ state.

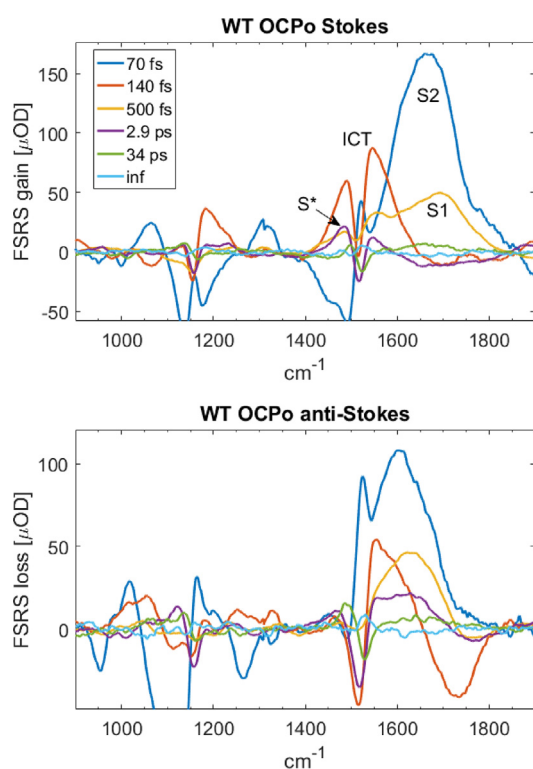


Figure 6. Stokes (A) and anti-Stokes (B) evolution associated decay (EAD) vibrational spectra of the OCP protein after excitation at 480 nm. Peak assignment is suggested for the Stokes EADS. This is a magnification of panels A2 and A3 from Figure 4, with the addition of the S_2 EADS and the assignments.

In a polar solvent, a slight broadening of the S_1 peak and a minor shortening of the last kinetic to 5 ps were observed. The first component in all experiments involving echinenone in solvents is associated with the typical absorbance of the S_2 state in the near-infrared region, which relaxes rapidly with an extremely short lifetime of 70 fs (blue). It decays into mixture of subsequent lower-lying excited states with 140 fs lifetime (red) consisting of a mixture of the S_2 state features and hot-ICT/ S_1 features. The 500 fs component (yellow) represents predominantly the hot S_1 state. In the case of echinenone dissolved in cyclohexane, there is only a single narrow band associated with the S_1 state, peaking at 591 nm, while in methanol (588 nm) and acetonitrile (583 nm), the S_1 peak coexists with a slight broadening in the lower energy region. This is known to be associated with the ICT state, typical for carbonyl carotenoids dissolved in polar solvents. The final components (magenta), 6 ps (cyclohexane) and 5 ps (methanol, acetonitrile), show the stabilized existence of the previously mentioned states^{1,54} S_1 and ICT, while ICT signature being almost negligible for echinenone in cyclohexane. In panels C1 and D1 of Figure 5, we also depict an “infinite” component, characterized by the presence of long living absorption in the infrared region,

which is likely associated with the formation of radicals due to undesired multi-photon transitions. The non-decaying signal appears exclusively for echinenone in polar solvents that help to stabilize the radical.

When comparing the absorption spectra of the excited states of echinenone in solvents with the OCPo, we observe significant differences in peak positions, shapes and lifetimes. This observation alone serves as evidence that the presence of echinenone within the protein greatly modulates its properties and the dynamics of excited states.

Our fitting results identify components with lifetimes of 70 fs, 140 fs, 500 fs, 2.9 ps, and 34 ps. These values align with the conclusions of a study by Nizinsky et al.⁵⁵; however, differences are noted at later lifetimes. Specifically, they observed two components. Instead of a 34 ps component, they resolved 5 and 80 ps components. This discrepancy can be explained if we assume that in our model only the 34 ps component is resolved being effectively a mixture of the 5 and 80 ps components reported by Nizinski et al.

The first component (70 fs – blue) is associated with absorption in the near-infrared region, corresponding to the S_2 state. The second component, which has a 140 fs lifetime (depicted in red), is believed to primarily represent the ICT state. In the OCPo protein, this component is characterized by two prominent bands, one around 670 nm and another around 750 nm. This observation does not align with data for echinenone in solvents, where the ICT state is almost entirely suppressed in cyclohexane or appears as a low-intensity shoulder in polar solvents. While one might be inclined to attribute the 670 nm band from OCPo to the S_1 state of echinenone and the 750 nm band to the ICT state, such an interpretation does not align with the FSRs data, as detailed in the FSRs results section. The third component, with a 500 fs lifetime (yellow), exhibits characteristics similar to the previous one (bands peaking at approximately 670 nm and 750 nm), but with the formation of a blue-shifted shoulder in the region around 580 nm. The fourth, 2.9 ps component (magenta), represents an evolution of the previously mentioned states, again with a pronounced band at 580 nm. In the literature,²⁹ this is known to be associated with the S^* state. Its significance in the OCP activation process is further explained in the FSRs results section and in the discussion. Interestingly, the final, fifth component of the OCPo TA (34 ps, depicted green) is characterized by the isolated presence of only this featureless single band around 580 nm, while the other bands have already relaxed. This result aligns with the findings reported in the literature^{29,55} where the final component of echinenone relaxation in OCPo is characterized by this band, identifying it as a potential precursor in the OCPo activation pathway. Likewise, at these

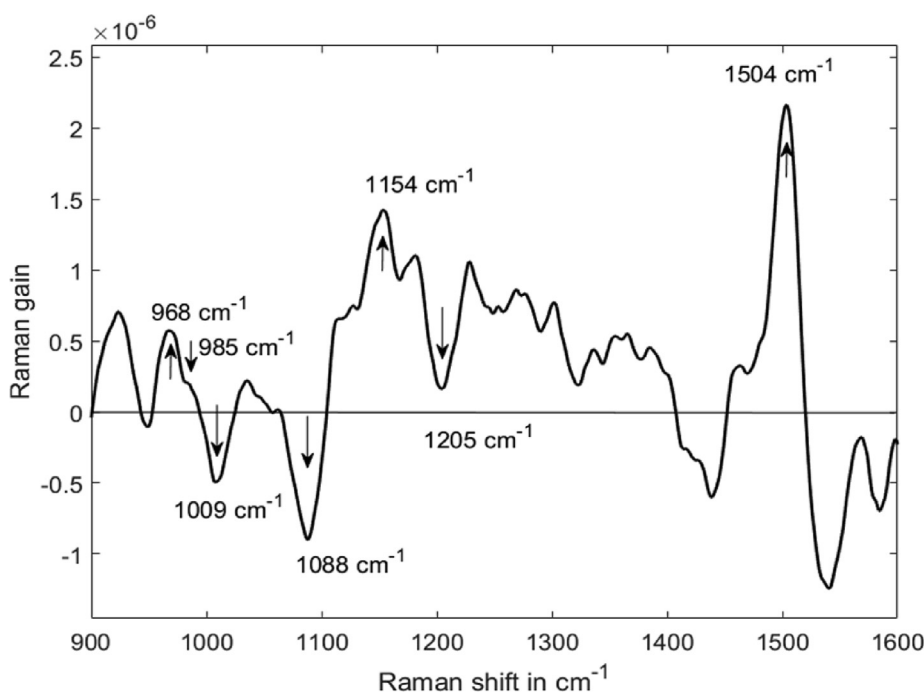


Figure 7. Transient FSRS spectra of the photoproduct formation. It is an average of data from 500 ps to 400 μ s delay interval originating from a different dataset than used to derive fs to ps components presented in the Figures 3–6. The data are the product of minimizing the OCPo GS component contribution so they represent relative changes compared to the normalized OCPo GS spectra rather than absolute value Raman spectra of the photoproduct.

delays, we no longer observe the presence of excited states of echinenone in experiments in pure solvents. Subsequently, only the radicals formed during the experiment are present (see the TA of echinenone in polar solvents, panels C1 and D1 of Figure 5). The data from the TA are correlated and discussed in the following section with the findings from the FSRS.

The following section presents a detailed comparison between the spectral characteristics of echinenone in various solvents and within OCPo, with a focus on the FSRS spectra analysis. The FSRS spectra of echinenone in solvents are visualized in the Figure 4, Stokes signals in subpanels B2, C2, D2 and anti-Stokes signals in subpanels B3, C3, D3. Complete FSRS spectra of OCPo are shown in the Figure 6 and for comparison with signals in solvents in the Figures 4 and 5, subpanels A2 (Stokes), A3 (anti-Stokes). The only difference between the Figure 4 and Figure 5 is scaling and removal of the ultrafast components in order to facilitate visualization of ps components that exhibit the most striking difference between vibrational dynamic of echinenone in solvents and in OCPo.

The initial component (blue) decays with a lifetime of 70 fs and is primarily associated with the S_2 state's C=C stretch. This is characterized in the Stokes spectra as a broad band extending from ~ 1550 cm^{-1} to 1800 cm^{-1} , with a center around 1640 cm^{-1} . In the anti-Stokes spectra, the band is

qualitatively similar. The appearance of the S_2 state is consistent with the literature.^{68,69}

The main distinction between S_2 state signature of echinenone in OCPo and in solvents, depicted in Figure S4, is that, in the OCPo experiment, the S_2 band is more clearly defined at these delays and is also broadened toward a region close to the 1517 cm^{-1} GS vibration, which, according to the literature,⁴³ is likely associated with the ICT state. This observation aligns with the findings in OCPo TA, where the S_2 absorption in the near IR region extends to approximately 650 nm, a range where ICT band is typically observed. The distinctive vibration features of the carotenoid in the protein might arise due to the more constrained environment of echinenone in OCP caused by the presence of the hydrogen bonds.

The second component, associated with a lifetime of 140 fs (depicted in red, Figure 6 for OCPo and Figure S4 for echinenone in solvents), is postulated to predominantly signify the ICT state in the case of echinenone in OCPo. In the FSRS data, both in the Stokes and anti-Stokes regions, a prominent ICT band at 1550 cm^{-1} is observed. Currently, in the TA of echinenone in OCPo, we observe the emergence of broad absorption as described earlier (peaking at 670 and 750 nm). As we have already hinted, it is challenging to attribute the peak at 670 nm to the S_1 state, since in the FSRS, we see very weak or no characteristics of this state. The negative

shoulder of the ICT band in the anti-Stokes signal likely arises from the re-pumping of the ICT state into the S_2 state via the Rp pulse, possibly supplemented by inversion in the vibration level population and resonance with ICT state stimulated emission. The generation of a superposition of vibrational coherences at various resonances is known to produce distorted peak shapes, in particular in the anti-Stokes frame (for details see “Peak shapes in FSRs spectroscopy” in the [Supporting information](#) and Refs. 70,71).

The third component, denoted in yellow and arising from a process with a lifetime of 500 fs, is predominantly associated with the coexistence of the ICT and hot S_1 states in both echinenone in solvents and in OCPo. In the FSRs signal from OCPo, the Stokes component features a prominent band peaking around 1700 cm^{-1} , extending asymmetrically towards lower wavenumbers. This observation aligns with the Morse potential approximation, where excited vibration states are more closely spaced and so red shifted, confirming the distinctive character of a hot S_1 state. Analogous to the preceding component, the anti-Stokes frame shows a superposition of the negative shoulder, likely stemming from vibration population inversion and possibly, to a lesser extent, from S_2 state re-pumping (for details see “Peak shapes in FSRs spectroscopy” in the [Supporting Information](#)). This latter effect is deemed less probable than at 140 fs, as the TA at 500 fs is already notably diminished at 790 nm, making any re-pumping induced by the Rp pulse minimal. While in echinenone in cyclohexane we mainly observe very similar features as in OCPo at this time scale, the experiment with echinenone in polar solvents show broad peak centered around 1650 cm^{-1} probably originating from a mixture of hot S_1 and ICT state.

The fourth (magenta) component, best visualized in [Figure 5](#), was fitted with a lifetime of ~ 3 ps in both TA and FSRs signals for OCPo and ~ 6 ps for echinenone in solvents. Its pronounced differences between OCPo and echinenone in various solvents, regardless of the solvent type, make it a central focus of this study. For echinenone in solution, this component, observed in both Stokes and anti-Stokes signals, features a distinct, sharp band peaking around 1775 cm^{-1} with only minor differences among solvents. Additionally, a less pronounced band around 1240 cm^{-1} was consistently recorded in all solvent datasets. These two modes serve as well-established indicators of the relaxed S_1 state of carotenoids, assigned to the blueshifted C=C and C—C modes, respectively.^{72,73} Notably, however, when echinenone is bound in OCPo, the C—C mode still appears around 1233 cm^{-1} , while the C=C mode at 1775 cm^{-1} is entirely absent in both Stokes and anti-Stokes frames. Instead, highly

pronounced bands emerge on the red edge of the GS bleach of C—C and C=C stretch, peaking around 1135 cm^{-1} and 1488 cm^{-1} , presumably originating from hot GS modes. This feature is not distinctly pronounced for echinenone in solution. Another surprising aspect is that for echinenone in solution, Stokes and anti-Stokes signals exhibit similar information, whereas in OCPo, the Stokes component predominantly features hot GS characteristics, while the anti-Stokes component displays ICT features not markedly different from those at 500 fs. This suggests that the relaxed ICT state has considerably less resonance at 790 nm in OCPo but retaining significant resonance at 700 nm where anti-Stokes resonance is effectively positioned. It's crucial to note that alongside the presence of hot GS modes, TA reveals the presence of a peak in the bluest part of the spectra (573 nm), previously identified as the S^* state signature. This correlation leads us to conclude that we are observing signatures of the same phenomenon.

As previously mentioned in the TA section on experiments in solvents, the fifth (green) component represents the spectra following the final relaxation of the excited state back to the ground state. The FSRs signal in polar solvents, where the solvent to echinenone ratio is unfavorable, is predominantly characterized by GS bleach. This is likely due to molecules that were photodamaged during the experiment and fail to recover. However, for echinenone in OCPo and cyclohexane, a distinct downshift in the C—C and C=C ground state stretches is observed, which presumably stems from the hot GS. In both OCPo and cyclohexane, the downshift of the C=C stretch peaks at 1494 cm^{-1} , indicating almost identical signatures in both OCPo and cyclohexane solutions. This downshift is noticeably smaller than that observed in the 3 ps component of OCPo, which not only shows a peak further in the red at 1488 cm^{-1} but also a tail that extends to much lower energies. This suggests that the hot GS observed in the 3 ps kinetics of OCPo is likely “hotter” indicating a population of higher vibrational states compared to cyclohexane.

The final blue component was exclusively fitted for OCPo. Within TA, it signifies the persistent radical amid various processes. In FSRs spectra, this component appears featureless. While this component may be expected to contain a photoproduct of early photoactivation, the available dataset lacked a sufficient signal-to-noise ratio at extended pump probe delays to overcome the minimal quantum yield of OCPo to OCP_r state photoconversion. Due to the substantial TA at 790 nm, especially within the initial 200 fs of TA, the Rp pulse induces notable sample degradation when probing these time scales by elevating the sample to unnatural higher-level states. Consequently, dedicated

experiments are favored to capture the photoproduct formation, avoiding probing of ultrafast processes. Although meaningful dynamics at the nanosecond to millisecond time scale couldn't be directly extracted, averaging measurements after 500 ps yielded spectra of the photoproduct, presented in Figure 7. These data originate from an experiment where the anti-Stokes region was not detected. The primary feature is a positive band at 1504 cm^{-1} with a slight negative feature at 1540 cm^{-1} , qualitatively aligning with the difference spectra between the OCPo and OCP_r shown in Figure 3, B2-3. We leave the deeper investigation of the early photoproduct dynamics for further studies.

Discussion

Three significant distinctions have emerged from the analysis of vibrational signals in optically excited echinenone across various solvents and in OCPo. Firstly, there are well resolved vibrational signatures of S_2 and ICT states during the initial 140 fs of carotenoid evolution. Secondly, a conspicuous absence of an established signature of the S_1 state, usually manifested as a narrow, blueshifted C=C stretch around 1775 cm^{-1} , in the OCPo. Thirdly, the OCPo exhibits more robust and enduring signatures of a vibrationally excited GS.

An investigation into potential causes and their implications for the photoactivation mechanism of OCPo is warranted. Notably, a brief S_2 state lifetime of approximately 70 fs was observed, a timescale considerably faster than typical vibration decoherence times observed for molecules at room temperature. The question arises as to whether such a short-lived state can exhibit a discernible vibrational signature. This inquiry hinges on the extent to which the molecular structure is defined in such a state. If significant structural rearrangements occur during the brief lifetime of this state, its vibrational spectra will be intricate and potentially lack distinct features. Conversely, stability during the ES prompts well-defined frequencies for vibrational modes, albeit constrained by the state's finite lifetime. The temporal energy uncertainty dictates an approximately 200 cm^{-1} full width at half maximum bandwidth for a 70-fs state, aligning well with the observed Raman band associated with the S_2 state in OCPo. This suggests that echinenone in solution might undergo rapid structural rearrangement that is restricted in OCPo as can be deduced from the more elusive Raman signature of the S_2 state in solution.

The second difference between OCPo and echinenone in solvents involves the absence of a clear S_1 state vibration population signature in OCPo. This complexity might arise due to distinct

conformations of echinenone in solvents and OCPo, where the end ring is in the trans configuration, and the effective conjugation length of echinenone in OCPo is thus slightly longer, contributing to a shorter S_1 state lifetime. Experiments reveal a clear signature of a hot S_1 state at 500 fs in both the Stokes and anti-Stokes regions, comparable to observations in cyclohexane. Notably, the S_1 state in OCPo appears somewhat hotter than in the solution, as evidenced by the broader vibrational peaks extending into lower energy modes. However, the signature of the relaxed S_1 state around 1775 cm^{-1} is not detected at all in OCPo, while it is very clear for echinenone in all studied solvents. This strongly suggests that no significant population of the relaxed S_1 state is formed, and such observation cannot be fully accounted for by the shortening of the lifetime compared to solvents. Target analysis of the TA data suggests that approximately 50 % of the S_1 state decays to the GS with a lifetime of 500 fs, and then approximately 75 % of the remaining S_1 population decays with a lifetime of 2.9 ps. It is important to note that we tested vibration signatures of OCP_r, and it shows the band of the relaxed S_1 state even though downshifted compared to echinenone in solution (cf. Figure S16). So, the observed lack of relaxed S_1 signatures is inherent to OCPo where the excited state dynamic appears to be ICT state dominated well beyond to what the echinenone molecule manifests even in the most ICT enhancing solvents.

The third difference pertains to the vibrational dynamics of the hot GS in OCPo. Comparative analysis with echinenone in solvents demonstrates a more pronounced redshift of the ground state C=C mode in 3 ps component in OCPo, indicating the formation of a much hotter form of GS vibrations. While signs of a hot S_1 state can be traced in the FSRs signals at the picosecond timescale in solvents, as mentioned above, no relaxed S_1 vibration is observed in OCPo. Instead, an unusually hot GS is formed, aligning with the timescale dominated by the S^* state in TA.

These combined results contribute to a hypothesis regarding the photoactivation mechanism of OCPo. The cooling dynamics of echinenone in OCPo and in solution are posited to be markedly different, as depicted in Figure 8. In solution, photon absorption likely triggers a structural conformational change associated with changes in bond length alteration.⁷⁴ This leads to major repositioning within the potential energy surface, possibly facilitating a transition to the S_1 state that might be favored after the conformational change. Also, a certain amount of energy can be dissipated during nuclear repositioning into solvent. Rapid S_1 state cooling at the 500 fs timescale forms a stable S_1 /ICT coupled population defined by an

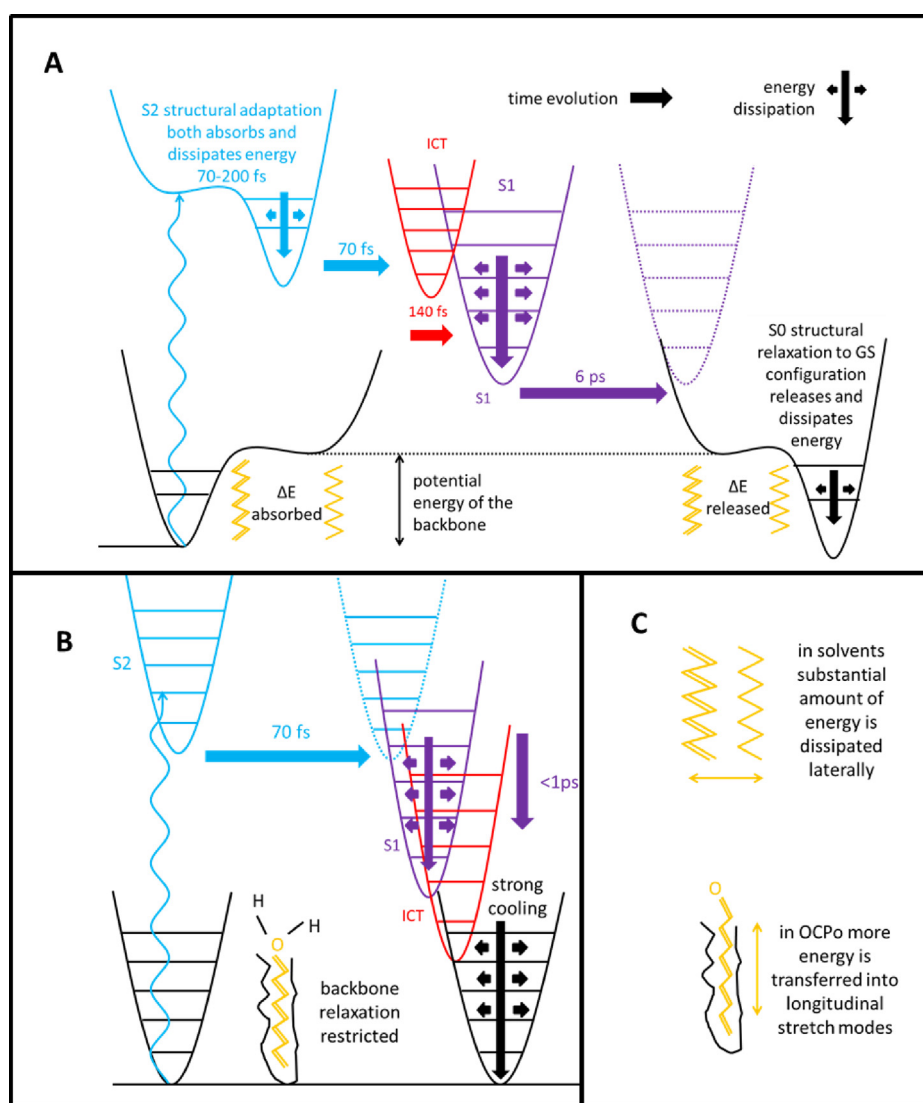


Figure 8. (A) Model of vibration cooling of echinenone in solvents. Energy is partially absorbed by structural adaptation to reduced bond alteration in the S_2 state. Later, additional energy is released during the S_1 state cooling. Only a fraction of the energy is released from the electronic ground state. (B) Model of vibrational relaxation in OCP. Sterical restriction and hydrogen bonds reduce the potential for conformational changes. Also, a very small S_1 population is formed. As a consequence, the hotter GS is formed with much higher levels of backbone C=C and C—C excitation. This results in more longitudinal changes of the backbone. C: Difference between conformational changes of carotenoid in solution and in OCP. In solution more lateral distortions are expected. Sterical restrictions in OCP lead to more energy in longitudinal modes.

blueshifted S_1 vibration mode at 1775 cm^{-1} and a small ICT band at 1620 cm^{-1} . After transitioning to the GS, potential energy is gradually released, resulting in only mildly hot GS vibrations. In contrast to that in OCPo, spatial constraints and hydrogen bonds on the keto group limit structural relaxation in the S_2 state, probably leading to an S_1 /ICT state strongly favoring the ICT configuration and a rapid transfer into the GS with an extraordinary level of C=C and C—C backbone stretch mode excitation. This funnels more energy into longitudinal modes, with less lateral dissipation. S^* was already suggested as a precursor of OCP photoactivation²⁹;

in this context, we confirm that with the observation that it is likely a form of unusually hot GS with its longitudinal modes excited in particular. Highly vibrationally excited modes of the backbone are thus suspected to be a precursor of photoactivation.

Conclusion

The comparison of vibrational signatures of the carotenoid echinenone in OCPo and organic solvents reveals distinctly different dynamics of energy dissipation following photon absorption. In solvents, the GS is achieved with only moderately

excited backbone C—C and C=C stretch modes, whereas in OCPo, the GS is formed with highly populated longitudinal stretching vibrational modes. Given that the formation and decay dynamics coincide with TA signatures previously assigned to the so-called S* state of echinenone, compelling evidence suggests that, at least in OCPo, the S* state is a form of an unusually hot electronic GS.

When comparing the vibrational definition of the echinenone S₂ state in solvents and OCPo, speculation arises that, in solvents, a substantial amount of energy is temporarily stored and dissipated through conformational changes, releasing a significant amount of energy laterally to the polyene backbone. It seems plausible that in a sterically restricted environment, such as a protein binding pocket, more energy remains in longitudinal stretching C=C and C—C modes. This enables the conversion of photon energy into nuclear motion directionally, transferring it into work, which, in the case of the OCPo protein, involves destabilization of the echinenone conformation in the binding pocket and facilitating the transition into OCPr.

Consequently, we propose that one driving mechanism behind OCPo photoactivation is the extraordinarily high level of excitation in longitudinal stretching modes of the carotenoid polyene backbone. This phenomenon appears to occur during both the excited and ground states, as unusually hot C=C stretch modes are observed in both cases. Highly excited backbone modes are expected to lead to bond length alteration triggering a conformational change. We propose that features observed in this work should be compared with structural data and density-functional calculations in the future.

CRedit authorship contribution statement

Petra Chrupková: Writing – review & editing, Writing – original draft, Data curation. **Ivo H.M. van Stokkum:** Software. **Thomas Friedrich:** Resources. **Marcus Moldenhauer:** Resources. **Nediljko Budisa:** Resources. **Hsueh-Wei Tseng:** Resources. **Tomáš Polívka:** Writing – review & editing. **Dmitry A. Cherepanov:** Writing – review & editing. **Eugene G. Maksimov:** Writing – review & editing. **Miroslav Kloz:** Writing – review & editing, Writing – original draft, Supervision, Project administration, Methodology, Investigation, Funding acquisition, Formal analysis, Data curation, Conceptualization.

DATA AVAILABILITY

Data will be made available on request.

DECLARATION OF COMPETING INTEREST

The authors declare that they have no known competing financial interests or personal relationships that could have appeared to influence the work reported in this paper.

Acknowledgment

TP thanks the Czech Science Foundation, grant No. 19-28323X, for financial support, M.K. was supported by the Czech Science Foundation (project No. 21-09692M and 21-05180S). EGM was supported by the Russian Science Foundation (grant number 23-14-00042). The authors are grateful for financial support by the SynCrop ETN consortium of the European Union (Horizon 2020 research and innovation program) under the Marie Skłodowska-Curie grant agreement No. 764591 (to HWT), by the Canada Research Chairs Program grant agreement No. 950-23197 (to NB), the German Research Foundation (grant no. 1276/6-1) and the Einstein Foundation Berlin for granting an Azura FPLC machine to TF.

Appendix A. Supplementary material

Supplementary material to this article can be found online at <https://doi.org/10.1016/j.jmb.2024.168625>.

Received 13 July 2023;

Accepted 17 May 2024;

Available online xxxx

Keywords:

OCP;
Raman;
spectroscopy;
ultrafast;
echinenone

References

- Polívka, T., Kerfeld, C.A., Pascher, T., Sundström, V., (2005). Spectroscopic properties of the carotenoid 3'-hydroxyechinenone in the orange carotenoid protein from the cyanobacterium *Arthrospira maxima*. *Biochemistry* **44**, 3994–4003.
- Wilson, A., Punginelli, C., Gall, A., Bonetti, C., Alexandre, M., Routaboul, J.M., Kerfeld, C.A., Van Grondelle, R., et al., (2008). A photoactive carotenoid protein acting as light intensity sensor. *Proc. Natl. Acad. Sci. U. S. A.* **105**, 12075–12080.
- Gwizdala, M., Wilson, A., Omairi-Nasser, A., Kirilovsky, D., (2013). Characterization of the *Synechocystis* PCC 6803 Fluorescence Recovery Protein involved in

- photoprotection. *Biochim. Biophys. Acta - Bioenerg.* **1827**, 348–354.
4. Kerfeld, C.A., Sawaya, M.R., Brahmamandam, V., Cascio, D., Ho, K.K., Trevithick-Sutton, C.C., Krogmann, D.W., Yeates, T.O., (2003). The crystal structure of a cyanobacterial water-soluble carotenoid binding protein. *Structure* **11**, 55–65.
 5. Leccese, S., Wilson, A., Kirilovsky, D., Spezia, R., Jolival, C., Mezzetti, A., (2023). Light-induced infrared difference spectroscopy on three different forms of orange carotenoid protein: focus on carotenoid vibrations. *Photochem. Photobiol. Sci.* **22**, 1379–1391.
 6. Sedoud, A., López-Igual, R., Rehman, A.U., Wilson, A., Perreau, F., Boulay, C., Vass, I., Krieger-Liszak, A., et al., (2014). The cyanobacterial photoactive orange carotenoid protein is an excellent singlet oxygen quencher. *Plant Cell* **26**, 1781–1791.
 7. Kirilovsky, D., (2007). Photoprotection in cyanobacteria: The orange carotenoid protein (OCP)-related non-photochemical-quenching mechanism. *Photosynth. Res.* **93**, 7–16.
 8. Kuznetsova, V., Dominguez-Martin, M.A., Bao, H., Gupta, S., Sutter, M., Kloz, M., Rebarz, M., Přeček, M., et al., (2020). Comparative ultrafast spectroscopy and structural analysis of OCP1 and OCP2 from *Tolypothrix*. *Biochim. Biophys. Acta – Bioenerg.* **1861**, 148120
 9. Sluchanko, N.N., Maksimov, E.G., Slonimskiy, Y.B., Varfolomeeva, L.A., Bukhanko, A.Y., Egorkin, N.A., Tsoraev, G.V., Khrenova, M.G., et al., (2024). Structural framework for the understanding spectroscopic and functional signatures of the cyanobacterial Orange Carotenoid Protein families. *Int. J. Biol. Macromol.* **254**, 127874
 10. Dominguez-Martin, M.A., Kerfeld, C.A., (2019). Engineering the orange carotenoid protein for applications in synthetic biology. *Curr. Opin. Struct. Biol.* **57**, 110–117.
 11. Piccinini, L., Iacopino, S., Cazzaniga, S., Ballottari, M., Giuntoli, B., Licusi, F., (2022). A synthetic switch based on orange carotenoid protein to control blue–green light responses in chloroplasts. *Plant Physiol.* **189**, 1153–1168.
 12. Andreoni, A., Lin, S., Liu, H., Blankenship, R.E., Yan, H., Woodbury, N.W., (2017). Orange carotenoid protein as a control element in an antenna system based on a DNA nanostructure. *Nano Lett.* **17**, 1174–1180.
 13. Leccese, S., Calcinoni, A., Wilson, A., Kirilovsky, D., Carbonera, D., Onfroy, T., Jolival, C., Mezzetti, A., (1871). Orange carotenoid protein in mesoporous silica: A new system towards the development of colorimetric and fluorescent sensors for pH and temperature. *Micromachines* **2023**, 14.
 14. Maksimov, E.G., Yaroshevich, I.A., Tsoraev, G.V., Sluchanko, N.N., Slutskaya, E.A., Shamborant, O.G., Bobik, T.V., Friedrich, T., et al., (2019). A genetically encoded fluorescent temperature sensor derived from the photoactive Orange Carotenoid Protein. *Sci. Rep.* **9**, 1–9.
 15. Pivato, M., Perozeni, F., Licusi, F., Cazzaniga, S., Ballottari, M., (2021). Heterologous expression of cyanobacterial Orange Carotenoid Protein (OCP2) as a soluble carrier of ketocarotenoids in *Chlamydomonas reinhardtii*. *Algal Res.* **55**, 1–23.
 16. Leccese, S., Onfroy, T., Wilson, A., Kirilovsky, D., Casale, S., Guira, S., Selmane, M., Jolival, C., et al., (2022). Immobilization of Orange Carotenoid Protein on mesoporous silica SBA-15 for the development of photoactivable nanodevices. *Microporous Mesoporous Mater.* **340**, 112007
 17. Kirilovsky, D., Kerfeld, C.A., (2013). The Orange Carotenoid Protein: A blue-green light photoactive protein. *Photochem. Photobiol. Sci.* **12**, 1135–1143.
 18. Punginelli, C., Wilson, A., Routaboul, J.M., Kirilovsky, D., (2009). Influence of zeaxanthin and echinenone binding on the activity of the Orange Carotenoid Protein. *Biochim. Biophys. Acta - Bioenerg.* **1787**, 280–288.
 19. Leverenz, R.L., Sutter, M., Wilson, A., Gupta, S., Thurotte, A., Bourcier de Carbon, C., Petzold, C.J., Ralston, C., et al., (2015). A 12 Å carotenoid translocation in a photoswitch associated with cyanobacterial photoprotection. *Science* **348**, 1463–1466.
 20. Gupta, S., Guttman, M., Leverenz, R.L., Zhumadilova, K., Pawlowski, E.G., Petzold, C.J., Lee, K.K., Ralston, C.Y., et al., (2015). Local and global structural drivers for the photoactivation of the orange carotenoid protein. *Proc. Natl. Acad. Sci. U. S. A.* **112**, E5567–E5574.
 21. Liu, H., Zhang, H., Orf, G.S., Lu, Y., Jiang, J., King, J.D., Wolf, N.R., Gross, M.L., Blankenship, R.E., (2016). Dramatic domain rearrangements of the cyanobacterial orange carotenoid protein upon photoactivation. *Biochemistry* **55**, 1003–1009.
 22. Bondanza, M., Cupellini, L., Lipparini, F., Mennucci, B., (2020). The multiple roles of the protein in the photoactivation of orange carotenoid protein. *Chem* **6**, 187–203.
 23. Dominguez-Martín, M.A., Sauer, P.V., Kirst, H., Sutter, M., Bina, D., Greber, B.J., Nogales, E., Polívka, T., et al., (2022). Structures of a phycobilisome in light-harvesting and photoprotected states. *Nature* **609**, 835–845.
 24. Yaroshevich, I.A., Maksimov, E.G., Sluchanko, N.N., Zlenko, D.V., Stepanov, A.V., Slutskaya, E.A., Slonimskiy, Y.B., Botnarevskii, V.S., et al., (2021). Role of hydrogen bond alternation and charge transfer states in photoactivation of the Orange Carotenoid Protein. *Commun. Biol.* **4**, 1–13.
 25. Tseng, H.-W., Moldenhauer, M., Friedrich, T., Maksimov, E.G., Budisa, N., (2022). Probing the spectral signatures of orange carotenoid protein by orthogonal translation with aromatic non-canonical amino acids. *Biochem. Biophys. Res. Commun.* **607**, 96–102.
 26. Moldenhauer, M., Tseng, H.W., Kraskov, A., Tavraz, N.N., Yaroshevich, I.A., Hildebrandt, P., Sluchanko, N.N., Hochberg, G.A., et al., (2023). Parameterization of a single H-bond in Orange Carotenoid Protein by atomic mutation reveals principles of evolutionary design of complex chemical photosystems. *Front. Mol. Biosci.* **10**, 1–13.
 27. Tsoraev, G.V., Bukhanko, A.Y., Mamchur, A.A., Yaroshevich, I.A., Sluchanko, N.N., Tseng, H.-W., Moldenhauer, M., Budisa, N., et al., (2023). Intrinsic tryptophan fluorescence quenching by iodine in non-canonical amino acid reveals alteration of the hydrogen bond network in the photoactive orange carotenoid protein. *Biochem. Biophys. Res. Commun.* **683**, 149119
 28. Bandara, S., Ren, Z., Lu, L., Zeng, X., Shin, H., Zhao, K.H., Yang, X., (2017). Photoactivation mechanism of a carotenoid-based photoreceptor. *Proc. Natl. Acad. Sci. U. S. A.* **114**, 6286–6291.
 29. Konold, P.E., Van Stokkum, I.H.M., Muzzopappa, F., Wilson, A., Groot, M.L., Kirilovsky, D., Kennis, J.T.M., (2019). Photoactivation mechanism, timing of protein

- secondary structure dynamics and carotenoid translocation in the orange carotenoid protein. *J. Am. Chem. Soc.* **141**, 520–530.
30. Wilson, A., Punginelli, C., Couturier, M., Perreau, F., Kirilovsky, D., (2011). Essential role of two tyrosines and two tryptophans on the photoprotection activity of the Orange Carotenoid Protein. *Biochim. Biophys. Acta - Bioenerg.* **1807**, 293–301.
 31. Maksimov, E.G., Protasova, E.A., Tsoraev, G.V., Yaroshevich, I.A., Maydykovskiy, A.I., Shirshin, E.A., Gostev, T.S., Jelzow, A., et al., (2020). Probing of carotenoid-tryptophan hydrogen bonding dynamics in the single-tryptophan photoactive Orange Carotenoid Protein. *Sci. Rep.* **10**, 1–12.
 32. Chukhutsina, V.U., Baxter, J.M., Fadini, A., Morgan, R.M., Pope, M.A., Maghlaoui, K., Orr, C.M., Wagner, A., et al., (2022). Light activation of Orange Carotenoid Protein reveals bicycle-pedal single-bond isomerization. *Nat. Commun.* **13**, 6420.
 33. Rose, J.B., Gascón, J.A., Sutter, M., Sheppard, D.I., Kerfeld, C.A., Beck, W.F., (2023). Photoactivation of the orange carotenoid protein requires two light-driven reactions mediated by a metastable monomeric intermediate. *Phys. Chem. Chem. Phys.* **25**, 33000–33012.
 34. Kish, E., Pinto, M.M.M., Kirilovsky, D., Spezia, R., Robert, B., (2015). Echinenone vibrational properties: From solvents to the orange carotenoid protein. *Biochim. Biophys. Acta - Bioenerg.* **1847**, 1044–1054.
 35. Mezzetti, A., Alexandre, M., Thurotte, A., Wilson, A., Gwizdala, M., Kirilovsky, D., (2019). Two-step structural changes in orange carotenoid protein photoactivation revealed by time-resolved Fourier transform infrared spectroscopy. *J. Phys. Chem. B* **123**, 3259–3266.
 36. Maksimov, E.G., Sluchanko, N.N., Slonimskiy, Y.B., Slutskaya, E.A., Stepanov, A.V., Argentova-Stevens, A. M., Shirshin, E.A., Tsoraev, G.V., et al., (2017). The photocycle of orange carotenoid protein conceals distinct intermediates and asynchronous changes in the carotenoid and protein components. *Sci. Rep.* **7**, 1–12.
 37. Ghosh, S., Bishop, M.M., Roscioli, J.D., Lafountain, A.M., Frank, H.A., Beck, W.F., (2016). Femtosecond heterodyne transient grating studies of nonradiative deactivation of the S2 (11Bu+) state of peridinin: Detection and spectroscopic assignment of an intermediate in the decay pathway. *J. Phys. Chem. B* **120**, 3601–3614.
 38. Polívka, T., Sundström, V., (2009). Dark excited states of carotenoids: Consensus and controversy. *Chem. Phys. Lett.* **477**, 1–11.
 39. Polívka, T., Sundström, V., (2004). Ultrafast dynamics of carotenoid excited states—from solution to natural and artificial systems. *Chem. Rev.* **104**, 2021–2071.
 40. Frank, H.A., Josue, J.S., Bautista, J.A., Van der Hoef, I., Jansen, F.J., Lugtenburg, J., Wiederrecht, G., Christensen, R.L., (2002). Spectroscopic and photochemical properties of open-chain carotenoids. *J. Phys. Chem. B* **106**, 2083–2092.
 41. Mirkovic, T., Ostroumov, E.E., Anna, J.M., van Grondelle, R., Govindjee, Scholes, G.D., (2017). Light absorption and energy transfer in the antenna complexes of photosynthetic organisms. *Chem. Rev.* **117**, 249–293.
 42. Di Donato, M., Ragnoni, E., Lapini, A., Foggi, P., Hiller, R. G., Righini, R., (2015). Femtosecond transient infrared and stimulated Raman spectroscopy shed light on the relaxation mechanisms of photo-excited peridinin. *J. Chem. Phys.* **142**, 212409
 43. Redeckas, K., Voiciuk, V., Vengris, M., (2016). Investigation of the S1/ICT equilibrium in fucoxanthin by ultrafast pump-dump-probe and femtosecond stimulated Raman scattering spectroscopy. *Photosynth. Res.* **128**, 169–181.
 44. Kosumi, D., Kusumoto, T., Fujii, R., Sugisaki, M., Inuma, Y., Oka, N., Takaesu, Y., Taira, T., et al., (2011). *J. Luminescence* **131**, 515–518.
 45. Zigmantas, D., Hiller, R.G., Sharples, F.P., Frank, H.A., Sundström, V., Polívka, T., (2004). Effect of a conjugated carbonyl group on the photophysical properties of carotenoids. *Phys. Chem. Chem. Phys.* **6**, 3009–3016.
 46. Chábera, P., Fuciman, M., Híbek, P., Polívka, T., (2009). Effect of carotenoid structure on excited-state dynamics of carbonyl carotenoids. *Phys. Chem. Chem. Phys.* **11**, 8795–8803.
 47. Khan, T., Litvín, R., Šebelík, V., Polívka, T., (2021). Excited-state evolution of keto-carotenoids after excess energy excitation in the UV region. *ChemPhysChem* **22**, 471–480.
 48. Kosumi, D., Kajikawa, T., Okumura, S., Sugisaki, M., Sakaguchi, K., Katsumura, S., Hashimoto, H., (2014). Elucidation and control of an intramolecular charge transfer property of fucoxanthin by a modification of its polyene chain length. *J. Phys. Chem. Lett.* **5**, 792–797.
 49. Enriquez, M.M., Fuciman, M., Lafountain, A.M., Wagner, N.L., Birge, R.R., Frank, H.A., (2010). The intramolecular charge transfer state in carbonyl-containing polyenes and carotenoids. *J. Phys. Chem. B* **114**, 12416–12426.
 50. Andersson, P.O., Gillbro, T., (1995). Photophysics and dynamics of the lowest excited singlet state in long substituted polyenes with implications to the very long-chain limit. *J. Chem. Phys.* **103**, 2509–2519.
 51. Gradinaru, C.C., Kennis, J.T.M., Papagiannakis, E., Van Stokkum, I.H.M., Cogdell, R.J., Fleming, G.R., Niederman, R.A., Van Grondelle, R., (2001). An unusual pathway of excitation energy deactivation in carotenoids: Singlet-to-triplet conversion on an ultrafast timescale in a photosynthetic antenna. *Proc. Natl. Acad. Sci. U. S. A.* **98**, 2364–2369.
 52. Balevičius, V., Abramavicius, D., Polívka, T., Galeštan Pour, A., Hauer, J., (2016). A unified picture of S^{*} in carotenoids. *J. Phys. Chem. Lett.* **7**, 3347–3352.
 53. Lenzer, T., Ehlers, F., Scholz, M., Oswald, R., Oum, K., (2010). Assignment of carotene S^{*} state features to the vibrationally hot ground electronic state. *Phys. Chem. Chem. Phys.* **12**, 8832.
 54. Šlouf, V., Kuznetsova, V., Fuciman, M., de Carbon, C.B., Wilson, A., Kirilovsky, D., Polívka, T., (2017). Ultrafast spectroscopy tracks carotenoid configurations in the orange and red carotenoid proteins from cyanobacteria. *Photosynth. Res.* **131**, 105–117.
 55. Niziński, S., Wilson, A., Uriarte, L.M., Ruckebusch, C., Andreeva, E.A., Schlichting, I., Colletier, J.P., Kirilovsky, D., et al., (2022). Unifying perspective of the ultrafast photodynamics of orange carotenoid proteins from synechocystis: Peril of high-power excitation, existence of different S^{*} states, and influence of tagging. *JACS Au* **2**, 1084–1095.
 56. Zigmantas, D., Hiller, R.G., Yartsev, A., Sundström, V., Polívka, T., (2003). Dynamics of excited states of the

- carotenoid peridinin in polar solvents: Dependence on excitation wavelength, viscosity, and temperature. *J. Phys. Chem. B* **107**, 5339–5348.
57. Takaya, T., Iwata, K., (2014). Relaxation mechanism of beta-carotene from S-2 (1B(u+)) state to Si (2A(g-)) state: Femtosecond time-resolved near-IR absorption and stimulated resonance Raman studies in 900–1550 nm Region. *J. Phys. Chem. A* **118**, 4071–4078.
 58. Mendes-Pinto, M.M., Sansiaume, E., Hashimoto, H., Pascal, A.A., Gall, A., Robert, B., (2013). Electronic absorption and ground state structure of carotenoid molecules. *J. Phys. Chem. B* **117**, 11015–11021.
 59. Mendes-Pinto, M.M., Galzerano, D., Telfer, A., Pascal, A. A., Robert, B., Iliaia, C., (2013). Mechanisms underlying carotenoid absorption in oxygenic photosynthetic proteins. *J. Biol. Chem.* **288**, 18758–18765.
 60. Yoshizawa, M., Kurosawa, M., (2000). Femtosecond time-resolved Raman spectroscopy using stimulated Raman scattering. *Phys. Rev. A - Mol. Opt. Phys.* **61**, 6.
 61. McCamant, D.W., Kukura, P., Yoon, S., Mathies, R.A., (2004). Femtosecond broadband stimulated Raman spectroscopy: Apparatus and methods. *Rev. Sci. Instrum.* **75**, 4971–4980.
 62. Umapathy, S., Lakshmana, A., Mallick, B., (2009). Ultrafast Raman loss spectroscopy. *J. Raman Spectrosc.* **40**, 235–237.
 63. Kloz, M., Weißborn, J., Polívka, T., Frank, H.A., Kennis, J.T.M., (2016). Spectral watermarking in femtosecond stimulated Raman spectroscopy: Resolving the nature of the carotenoid S^{*} state. *Phys. Chem. Chem. Phys.* **18**, 14619–14628.
 64. Andrikopoulos, P.C., Liu, Y., Picchiotti, A., Lenngren, N., Kloz, M., Chaudhari, A.S., Precek, M., Rebarz, M., et al., (2020). Femtosecond-to-nanosecond dynamics of flavin mononucleotide monitored by stimulated Raman spectroscopy and simulations. *Phys. Chem. Chem. Phys.* **22**, 6538–6552.
 65. Maksimov, E.G., Moldenhauer, M., Shirshin, E.A., Parshina, E.A., Sluchanko, N.N., Klementiev, K.E., Tsoraev, G.V., Tavraz, N.N., et al., (2016). A comparative study of three signaling forms of the orange carotenoid protein. *Photosynth. Res.* **130**, 389–401.
 66. Leverenz, R.L., Jallet, D., Li, M.-D., Mathies, R.A., Kirilovsky, D., Kerfeld, C.A., (2014). Structural and functional modularity of the orange carotenoid protein: Distinct roles for the N- and C-terminal domains in cyanobacterial photoprotection. *Plant Cell* **26**, 426–437.
 67. Prince, R.C., Frontiera, R.R., Potma, E.O., (2017). Stimulated Raman scattering: From bulk to nano. *Chem. Rev.* **117**, 5070–5094.
 68. Kukura, P., McCamant, D.W., Mathies, R.A., (2004). Femtosecond time-resolved stimulated Raman spectroscopy of the S 2 (1B u+) excited state of β-carotene. *J. Phys. Chem. A* **108**, 5921–5925.
 69. Takaya, T., Iwata, K., (2014). Relaxation mechanism of β-carotene from S2 (1B u+) state to S1 (2Ag-) state: Femtosecond time-resolved near-IR absorption and stimulated resonance Raman studies in 900–1550 nm region. *J. Phys. Chem. A* **118**, 4071–4078.
 70. Dobryakov, A.L., Krohn, O.A., Quick, M., Ioffe, I.N., Kovalenko, S.A., (2022). Positive and negative signal and line shape in stimulated Raman spectroscopy: Resonance femtosecond Raman spectra of diphenylbutadiene. *J. Chem. Phys.* **156**, 084304
 71. Oscar, B.G., Chen, C., Liu, W., Zhu, L., Fang, C., (2017). Dynamic Raman line shapes on an evolving excited-state landscape: Insights from tunable femtosecond stimulated Raman spectroscopy. *J. Phys. Chem. A* **121**, 5428–5441.
 72. Hashimoto, H., Koyama, Y., (1989). Raman spectra of all-trans-β-carotene in the S1 and T1 states produced by direct photoexcitation. *Chem. Phys. Lett.* **163**, 251–256.
 73. McCamant, D.W., Kukura, P., Mathies, R.A., (2003). Femtosecond time-resolved stimulated Raman spectroscopy: Application to the ultrafast internal conversion in β-carotene. *J. Phys. Chem. A* **107**, 8208–8214.
 74. Accomasso, D., Arslançan, S., Cupellini, L., Granucci, G., Mennucci, B., (2022). Ultrafast excited-state dynamics of carotenoids and the role of the SXState. *J. Phys. Chem. Lett.* **13**, 6762–6769.